Influence of an Oscillating Airflow on the Prefilming Airblast Atomization Process

Thomas Christou*, Björn Stelzner, Nikolaos Zarzalis
Engler-Bunte-Institute, Division of Combustion Technology
Karlsruhe Institute of Technology
Karlsruhe, Baden-Württemberg, 76131, Germany

Abstract

Thermoacoustic instabilities often occur in a combustion chamber of a jet engine when pressure fluctuations from the released heat create a closed feedback loop with the fluctuations of the inlet air velocity, causing further combustion instabilities that enhance the cycle back again. Since most jet engine combustion chambers use liquid fuel dispersed into droplets by an airblast atomizer, any fluctuations occurring in the air entering the airblast nozzle could affect the atomization process of the liquid fuel and the air to fuel ratio distribution inside the combustor. The present experimental study focuses on the influence of the pulsating airflow on the spray characteristics during the airblast atomization process. The experiments were carried out with a two-dimensional prefilmer in which a water film flow was generated on one surface. A siren excited the airflow at approximately 120 Hz. The oscillation of the airflow was characterized by a Constant Temperature Anemometer, while the developed spray was examined using Phase Doppler Anemometry where droplet velocities and the droplet size distribution were measured. By processing the droplet characteristics, an oscillation of the mean diameter, Sauter Mean Diameter and droplet velocity is observed. In comparison to a non-forced flow case as well as theoretical predictions of the SMD based on the air velocity, these results may indicate that the oscillating air velocity causes a time-dependent separation of the droplets which results in those fluctuating spray characteristics.

Keywords: airblast atomization, thermoacoustics, instabilities, jet engine

Nomenclature

b	Liquid film width	$[mm]$
D	Diameter	$[\mu m]$
D_{10}	Mean Diameter	$[\mu m]$
D_{32}	Sauter Mean Diameter	$[\mu m]$

*Corresponding author: Thomas.Christou@partner.kit.edu

f	Frequency	$[Hz]$
h	Prefilming edge thickness	$[\mu m]$
N	Rotational speed	$[RPM]$
Re	Reynolds Number	$[-]$
t	Time	$[s]$
T	Time period	$[ms]$
u	Velocity	$[m/s]$
$\bar{u}_g$	Mean gas velocity	$[m/s]$
$\bar{u}_d$	Mean droplet velocity	$[m/s]$
$\dot{V}/b$	Film loading	$[mm^2/s]$
$\dot{V}$	Volume flow rate	$[m^3/s]$
We	Weber number	$[-]$

Greek

$\delta_{x,e}$	Boundary layer thickness	$[mm]$
$\Delta( )$	Difference	$[-]$
Δx	Infinitesimal liquid film width	$[mm]$
ρ	Density	$[kg/m^3]$
φ	Phase angle	$[°]$

Subscripts

$()_d$	Droplet
$()_g$	Gas
$()_l$	Liquid

Acronyms

ALR	Air-to-Liquid Ratio
CTA	Constant Temperature Anemometer
FFT	Fast Fourier Transform
LPP	Lean Premixed Prevaporized

NACA	National Advisory Committee for Aeronautics
PDA	Phase Doppler Anemometry
SMD	Sauter Mean Diameter
TUM	Technical University of Munich

1. Introduction

To achieve the goals of clean combustion technology for aircraft engines by reducing harmful emissions, the major jet engine manufacturers are developing lean premixed prevaporized (LPP) combustion chamber designs that operate at high pressures. In this LPP context, thermoacoustic instabilities often occur in the combustion chamber when pressure oscillations from the released heat by the flame create a feedback loop with the inlet air velocity (Dowling and Stow, 2003). These high-pressure oscillations carry a high risk for reduced robustness and lifetime of the engines (DeLaat and Paxson, 2008). Since modern combustion chambers use prefilming airblast atomizers to atomize the liquid fuel into droplets, oscillating behavior of the air entering the air blast nozzle also causes disturbances of the air-to-liquid ratio (ALR), i.e. the ratio of air mass flow rate over liquid mass flow rate, which affects the pressure drop across the nozzle. Since the pressure drop across the nozzle is a dominant factor in the atomization process of the air jet (Gurubaran et al., 2008), possible fluctuations of the air-to-liquid ratio affect the generated spray. It is therefore relevant to predict the instabilities in the droplet characteristics during these phenomena.

Similar studies concerning a generic prefilming airblast atomizer have been conducted (Müller et al., 2006; Inamura et al., 2012; Déjean et al., 2013), while the acoustic response of the generated spray under forced flow conditions has also been investigated (Müller et al., 2006; Chaussonnet et al., 2017; Eckstein et al., 2005; Gajan et al., 2007). The Sauter Mean Diameter (SMD) of the spray is shown to be strongly affected at low frequencies, while at higher frequencies there seems to be no significant effect, showing a low-pass behavior (Chaussonnet et al., 2017).

To predict the fluctuations in the spray characteristics, Phase Doppler Anemometry (PDA) was used in this study in order to track the velocity and the diameter of the droplets, while hot wire anemometry was applied to measure the air velocity. The resulted signals were phase-averaged for one period of the phenomenon, providing a clear depiction of the oscillation according to the forced frequency. In the first part of the paper, the experimental setup and measurement techniques are described, followed by the discussion regarding the measured results and finally the conclusion with the summary of the outcomes from this work.

2.Experimental Setup

On the above-mentioned test rig, which is schematically shown in Figure 1, the main airflow is divided into two different channels. A certain amount of the total air mass flow passes the siren and is excited at certain frequencies before being mixed with the rest of the mass flow, which is bypassed through an air plenum.

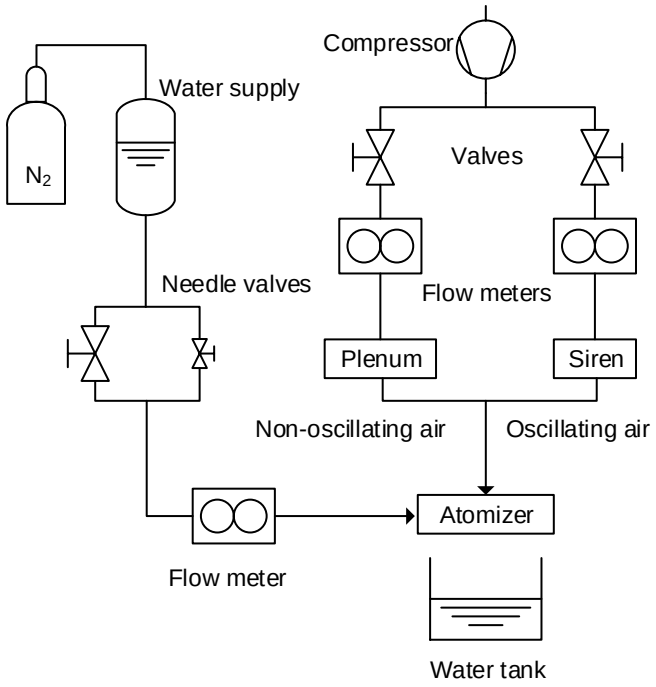

Figure 1. Experimental setup schematic.

After the mixing, the total air flows through a 1.5 m resonance tube before reaching the airblast prefilmer nozzle at atmospheric pressure. The liquid (water in the present work) is fed into the system from a pressurized vessel and is controlled by two independent needle valves. Finally, the water is collected in a tank after being atomized into spray at the prefilming airblast nozzle.

2.1.Airblast atomizer configuration

The designed and manufactured airblast atomizer presented in Figure 2 is similar to the design developed by Müller et al. (Müller et al., 2006). It consists of a standardized symmetrical airfoil profile (NACA-0010) made of stainless steel with a chord length of 73 mm and a trailing edge thickness, i.e. an atomizing lip thickness of about 200 μm. The cavity on the inside hosts the liquid, which then exits through 40 equidistant holes on the surface of the prefilmer, creating a uniform liquid film. The water is entering the cavity on the inside of the prefilmer symmetrically from the two sides before it reaches the surface flowing through the 40 holes. The air flows on both sides

of the prefilming atomizer, while the liquid film covers only the one side, thus reproducing the prefilm surface of a conventional airblast atomizer.

For planar model atomizers of this type, it is suggested that the liquid flow rate be expressed in terms of film load $\dot{V}/b$ in units of mm²/s (Müller et al., 2006); this implies the absence of the width of the liquid film b and the liquid's density ρ. The former has the effect that the flow rate refers to a two-dimensional flow in one slice (of an infinitesimal depth Δx) of the prefilming surface, while the latter allows the comparison with other types of liquid. This way, as shown in Figure 3, the flow rate of the generic nozzle can be compared to a realistic design of an airblast atomizer.

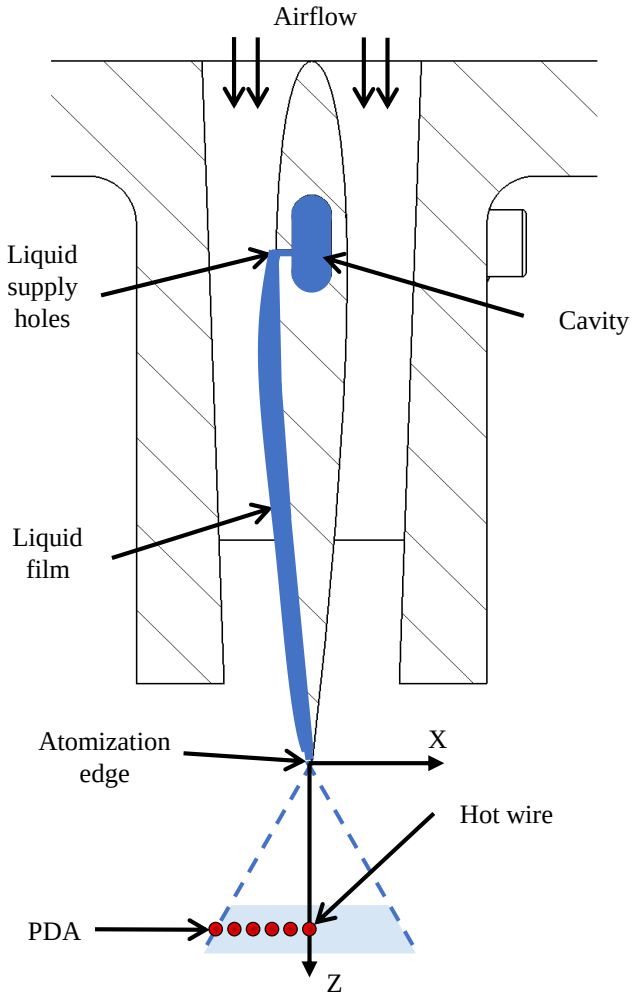

Figure 2. Schematic representation of the prefilming airblast atomizer and the measurement positions.

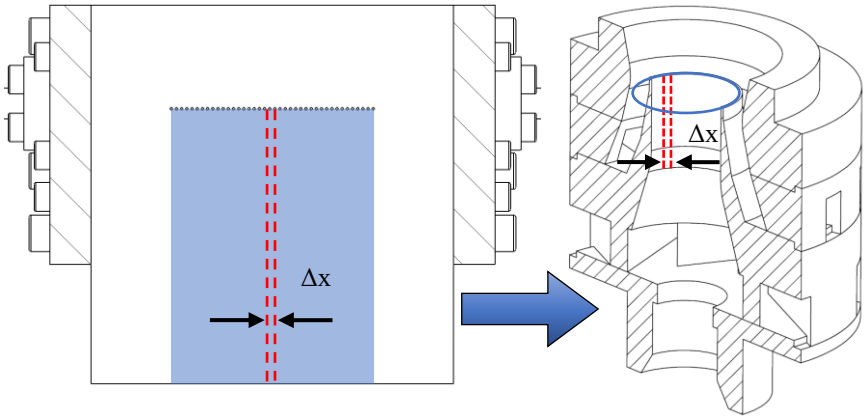

Figure 3. Comparison of model atomizer with typical airblast atomizer.

2.2.Pulsating flow generator

Part of the total air mass flow passes through the siren and is excited with frequencies up to 800 Hz. The siren used for air excitation (Figure 4) was designed and manufactured at the Technical University of Munich (Eckstein et al., 2005). It consists of a housing with an internal rotating disc attached to a motor whose speed is controlled by computer software. The rotor and the fixed housing have eight and four openings, respectively, through which the air can flow. During rotation of the rotor, when the openings of the rotor coincide with the stationary openings of the siren housing the air passes through, otherwise the flow is interrupted. Therefore, the air flows at forced frequency, which is linearly dependent on the rotational speed of the siren rotor:

$$f = \frac{8}{60} N \tag{1}$$

where f is the frequency in Hz at which the air is allowed to pass through and N the rotational speed of the motor in RPM, regulated by the software.

2.3.Bypass plenum

The rest of the total air mass flow passes through the bypass plenum. As shown in Figure 4, the air is inserted tangentially in the plenum through two pipes and then flows through 24 drilled holes coaxially with siren and the resonance tube in order to mix with the pulsating flow coming from the siren. The inlet pipes have been designed with a relatively large effective area (inner diameter of Ø39 mm) and holes with an optimum length to diameter ratio of two in order to max-

imize the discharge coefficient and thus minimize the pressure drop across the plenum. The resulting airflow after mixing was studied at the end of the resonance tube, where the model of the prefilming airblast atomizer was placed.

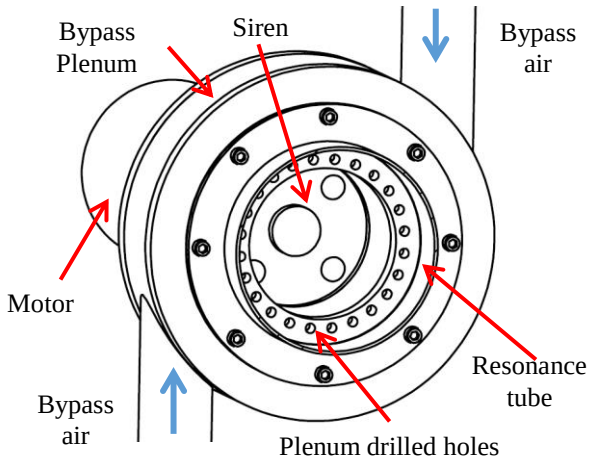

Figure 4. Configuration of siren and bypass plenum prior to the 1.5 m resonance tube and the airblast atomizer.

3.Measurement techniques

The airflow velocity and its fluctuation over time due to the siren were measured by hot wire Constant Temperature Anemometry (CTA), using a single-wire platinum hot film probe of 50.8 μm diameter and 1.02 mm length. The data rate chosen for the operation of this device was 20 kHz.

The hot wire probe was placed inside the air duct of the prefilmer in the middle of the duct (35 mm from both sides) and 40 mm downstream of the atomization edge (shown in Figure 2) in order to characterize the airflow forced by the siren.

The characterization of the spray, i.e. the droplet velocity and diameter, was carried out using a commercial Phase Doppler Anemometry (PDA) system in first-order refraction mode, in a setup with a three-detector receiving optic at a scattering angle of 30°. For the vertical velocity component and the diameter measurement, the green line with a wavelength of 532 nm from a diode-pumped solid-state laser (2x150 mW) was utilized. For both the sending and receiving fiber optics, lenses with a focal length of 500 mm were used. This setup configuration involves an effective spatial filter width of 0.4 mm, phase factors of 2.212 °/μm and 0.8679 °/μm for detectors 1-2 and 1-3 respectively, enabling for droplet diameter measurements up to approximately 300 μm. When the measurement volume was located inside the region of the dense spray, data rates of 5 to 10 kHz

were achieved, with a validation rate of approximately 60%. This relatively high data rate is a crucial factor for tracking the possible fluctuations that may appear in the characteristics of the spray.

Preliminary measurements using shadowgraphy imaging technique showed that large ligaments appear up to about 4 mm downstream of the prefilmer edge. Therefore, for the PDA measurements a ten times larger safety distance, i.e. at 40 mm, was selected, while a scan of six positions along the X-axis (-10 mm to 0 mm) was also accomplished in order to investigate the influence of the air modulation on the spray characteristics in space (Figure 2). Regarding the Y-axis, which is perpendicular to the plane shown in Figure 2, preliminary measurements had shown that the spray is acceptably uniform, therefore the selected positions are taken in the center of the prefilmer along the Y-axis.

The forced flow measurements were carried out at the frequency determined during siren characterization. On the other hand, a non-forced flow measurement was performed at an airflow velocity corresponding to the average of the forced flow experiment's velocity, thus enabling a comparison between the two cases. Naturally, in all of the aforementioned experiments, the film loading on the prefilmer was kept constant at 83.5 mm^2/s.

4.Results

4.1.Siren characterization

In order to characterize the operation of the siren in terms of amplitude and frequency, CTA hot wire measurements were carried out. After calibrating the probe for the expected velocity range, the first step was to measure the air velocity at the nozzle while the siren is in operation. While maintaining the same mass flow through the siren and a certain split ratio between the siren and the plenum, the flow velocity fluctuations were measured for each rotational speed of the motor. To investigate the effect of different rotational speeds on the flow at constant total air mass flow and air split ratio, the target range was set around $f = 120$ Hz, or $N = 900$ RPM according to Equation 1. The measurements were carried out for 21 different rotational speeds, starting from 700 RPM to 1100 RPM, with an increment of 20 RPM. The measurements were performed at a sampling rate of 20 kHz, which is sufficient to characterize the phenomena with expected frequencies around 120 Hz, for a duration of 13.1 s per local point. After the velocity measurements were

accomplished, it is essential to analyze the results in the frequency domain, via a Fast Fourier Transform (FFT).

Figure 5 shows the FFT of the 21 velocity signals measured 40 mm downstream of the prefilmer at the center of the nozzle, depending on excitation frequency (each different curve representing a measurement with one corresponding rotational speed). The amplitude of the oscillation of each signal is represented by the dashed line connecting the peaks of the different curves, which shows that the highest resonance occurs around 114 Hz for the same mass flow. It is worth mentioning that the dotted vertical black lines, which represent the theoretical frequency that should occur as a function of the forced rotational speed according to Equation 1, strictly follow the calculated frequencies with a maximum deviation of less than 0.20 Hz.

For the present work, the rotational speed of 900 RPM was chosen for the operation of the siren in order to investigate the atomization process, which corresponds to $f = 120$ Hz as calculated from Equation 1, or 120.16 Hz as measured with the hot wire anemometry and calculated through the FFT. At all the rotation speeds tested, the higher harmonics had a non-zero but negligible amplitude.

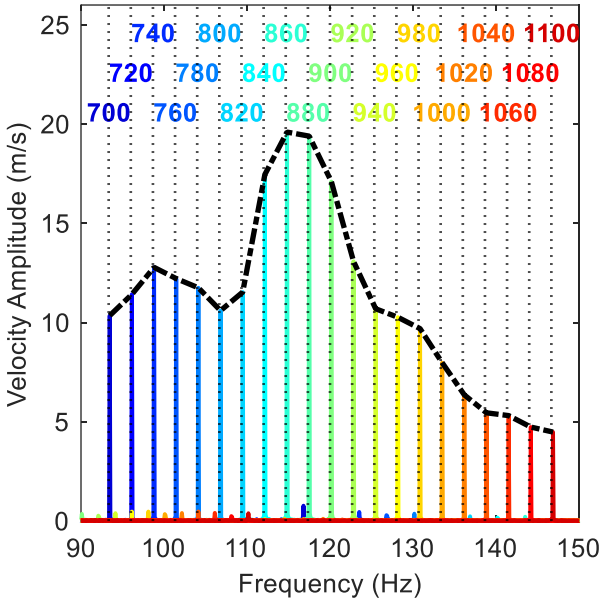

Figure 5. FFT of the air velocity measured inside the prefilmer for 11 different rotational speeds of the siren in RPM, showing the resonance around 114 Hz.

Since the frequency appearing on the signal is determined by FFT, it is possible to calculate a phase averaged velocity signal from all the separate periods included in it. Each point can be averaged with its counterpart in all the other periods, with a time step of exactly $T = 1/f = 8.32$ ms (i.e. a time step equal to the period of the determined excitation frequency).

In Figure 6 the result of this method is shown; the solid line is the resulting phase averaged velocity for one period (corresponding to one-eighth of the rotation of the siren rotor), while the mist of lines on the background illustrates all the separate one-period signals, one on top of the other. The resulting curve after the phase averaging shows a negligible deviation from all the separate periods contained in the signal, indicating how accurately the siren produces the oscillation in the flow without interferences in the signal. In fact, the maximum deviation of the original signal from the phase-averaged result is less than 8% at the extrema of the fluctuation.

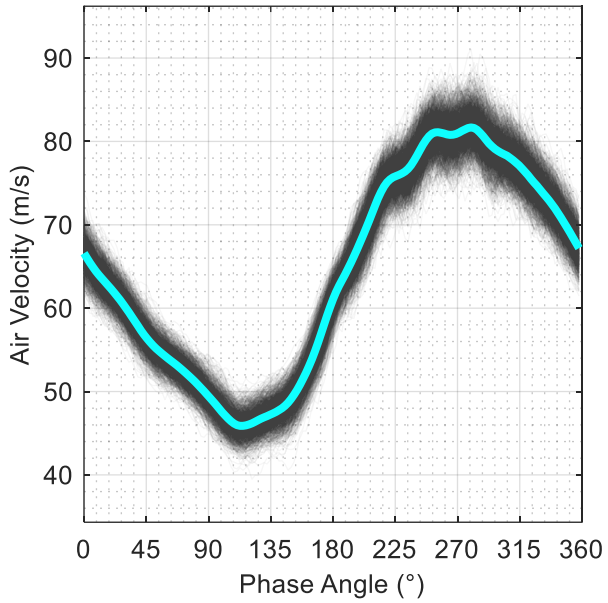

Figure 6. Phase averaging of velocity signal measured 40 mm downstram of the prefilmer at an excitation frequency of 120.16 Hz.

4.2.Forced flow – single position analysis

In order to measure the spray characteristics with PDA, starting at the center of the spray shown in Figure 2, it is necessary to operate the siren at the rotational speed that was determined through the aforementioned analysis. At the same time, the same airflow split and the same average total air mass flow were maintained. While the air was excited by the siren with a frequency of $f = 120.16$ Hz, the influence on the atomization process was recorded with PDA measurements.

For each droplet passing through the measurement volume, its velocity, as well as its diameter, was measured with its according time stamp. By post-processing the 100,000 samples of droplet data in a MATLAB code which was developed for this purpose, it was possible to derive their periodic fluctuation as a function of the phase angle, similarly to how the phase-averaged velocity of the air was calculated. The basic characteristics of the spray were averaged in twenty bins for a time period that corresponds to one period of the phenomenon.

Figure 7 shows the phase-averaged mean diameter of the spray, where a significant fluctuation of approximately 20% of its average value is observed. On the same graph, the number of droplets passing by the measurement volume is shown, which seems to oscillate unevenly around its average value. The sudden increase in the droplet number until the phase of 270° matches the drop of the mean diameter. Another way of explaining this behavior is by observing the original diameter data of each individual droplet along one period of the oscillation, in Figure 8. The droplet number is again illustrated along the period as the number density in a grid on top of the diameter data. It is evident that the increase of droplet number around 270°mainly concerns droplets of smaller diameters, therefore the mean droplet diameter is decreasing. Simultaneously, the oscillation of the SMD along the period is shown in Figure 8, which matches in phase the mean diameter.

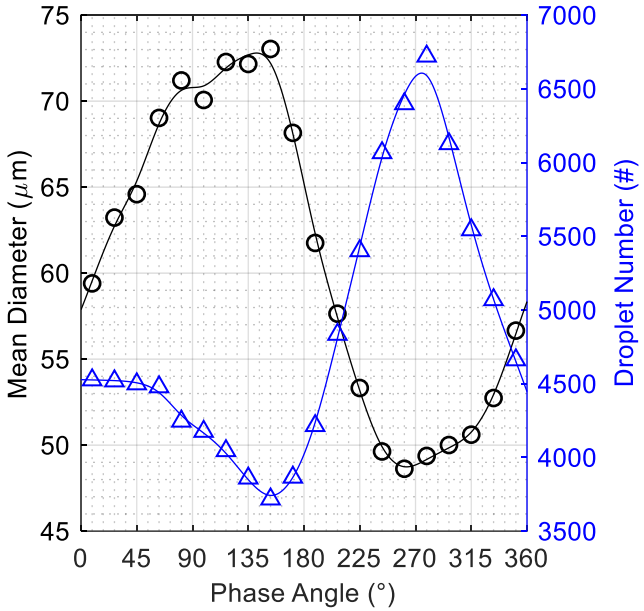

Figure 7. Phase averaging of D_{10} and droplet number at 120.16 Hz.

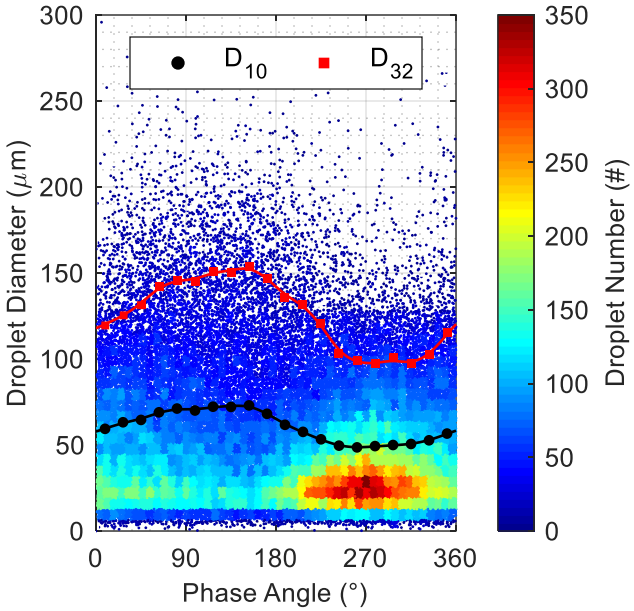

Figure 8. Droplet diameter – number density along one period at 120.16 Hz.

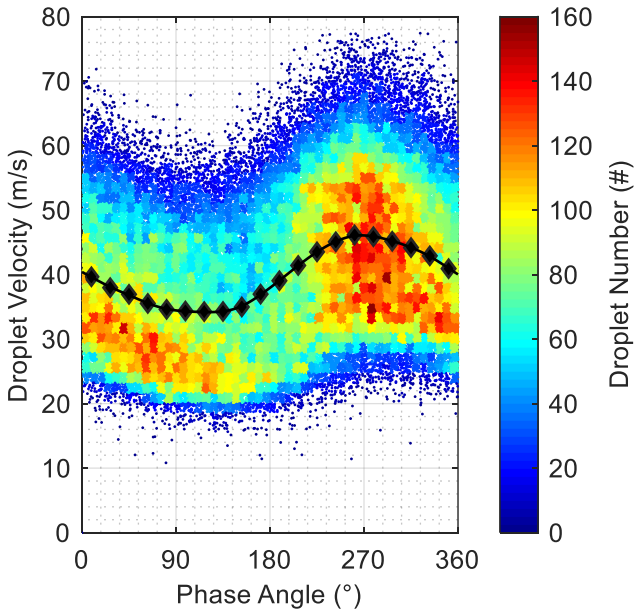

Figure 9. Droplet velocity – number density along one period at 120.16 Hz.

Apart from the diameter information, the velocity of each droplet was calculated through the PDA technique. In Figure 9, the velocities of all detected droplets are illustrated when each measured droplet is placed in its corresponding timestamp for one period, while the phase-averaged droplet velocity is shown as well in a black curve. The density in the velocity of the droplets is also illustrated in Figure 9 during the period of oscillation, simultaneously with the independent

velocity of each droplet. It is evident that during a certain part of the period (i.e. around 270° according to the current reference for the start) more droplets than average pass through the measurement volume. This was already clear in Figure 7, but Figure 9 shows that this burst of droplets around 270° is divided into many different velocities, which further means a variety of droplet diameters.

In order to have a better overview of the mean droplet velocity, the droplets were divided into size classes according to their diameter. In Figure 10, this size-class separation is shown for sixteen diameter classes (up to 160 μm), phase-averaged in one period, along with the phase-averaged velocity of all the droplets in the black curve. As expected, the small droplets have a higher velocity because they are better able to follow the trajectory of the airflow due to their low inertia and a subordinate small Stokes number (Collins and Keswani, 2004). With increasing droplet diameter the mean droplet velocity has a lower mean value and a lower oscillation amplitude. The velocities on the classes of the largest droplets seem to converge, one above the other, matching the minimum values of droplet velocities from Figure 9.

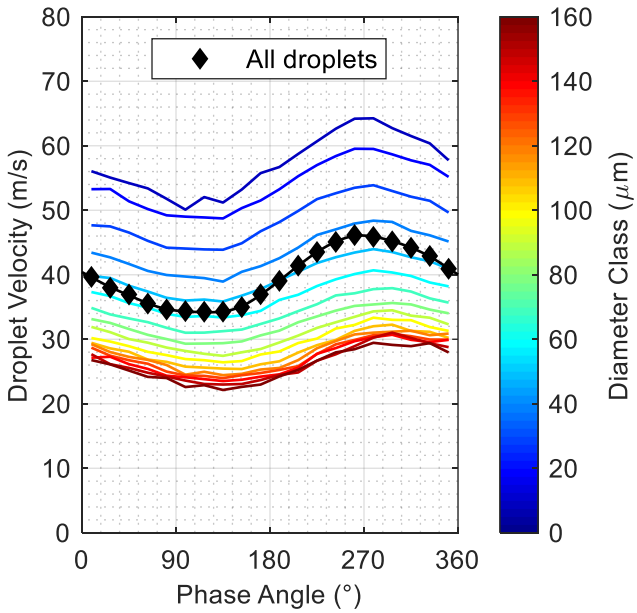

Figure 10. Size-class separation for the phase averaged mean droplet velocity at 120.16 Hz.

To conclude with the single position characterization of the spray, the final parameter that needs to be observed is how the SMD of the spray oscillates during the period (Figure 11), briefly discussed already regarding Figure 8. Two main outcomes are observed apart from the fact that the SMD also fluctuates over the period. The first is that there is a natural shift of approximately

180° between the droplet velocity (Figure 9) and the SMD (or the mean diameter from Figure 7), as shown by other similar investigations as well (Müller et al., 2006), because the smaller the droplets, the faster they move. The second outcome becomes apparent when the SMD of a non-forced experiment at the average air velocity of Figure 6 is displayed simultaneously with the SMD of the forced flow case. The SMD of the mean air velocity is almost the same as the mean SMD of the forced case, namely slightly lower.

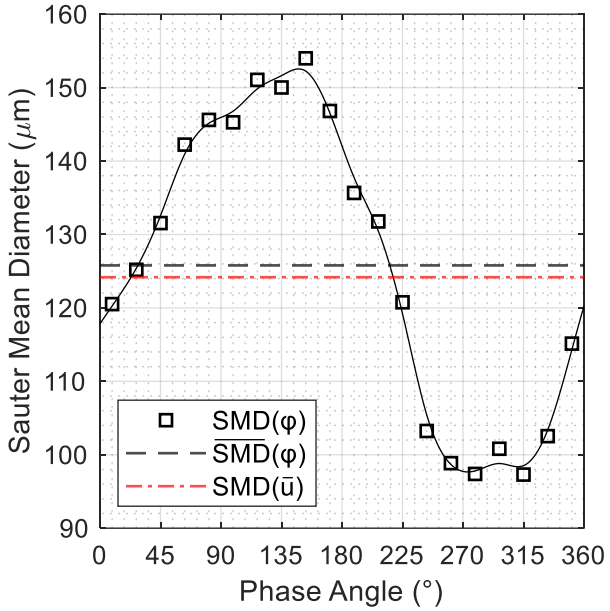

Figure 11. Phase averaging of SMD at 120.16 Hz in comparison with unforced flow SMD.

This could indicate that the spray in the two cases of a forced flow and a stationary flow at the average forced air velocity is similar because of the breakup mechanism, but the droplets are subject to a temporal separation. To further support the hypothesis of this separation of the droplets, a similar behavior concerning the average SMD can be noticed numerically by using the following model (Gepperth et al., 2012):

$$\frac{D_{32}}{\delta_{x,e}} = 4.96\, Re_d^{-0.17}\, We_d^{-0.36} \left(\frac{\rho_l}{\rho_g}\right)^{-0.013} \left(\frac{h}{\delta_{x,e}}\right)^{0.46} \tag{2}$$

With this model it is possible to directly correlate the SMD with the gas velocity as follows:

$$D_{32} = c \cdot\, u_g^{-0.892} \tag{3}$$

where c is a constant derived from all the constants and the gas and liquid properties of Equation 2.

The SMD calculated from Equation 3 fluctuates asymmetrically about its mean value if the gas velocity is forced to follow the phase-averaged velocity shown in Figure 6. This is observed in

Figure 12, which simultaneously shows the measured phase-averaged air velocity and the calculated SMD, as well as the average SMD and the SMD of the average air velocity. According to Equation 3, the SMD of the average air velocity is 115.7 µm, while the average SMD of the oscillating solution from Equation 3 is slightly higher at 119.5 µm, reflecting the behavior observed in the experimental results in Figure 11.

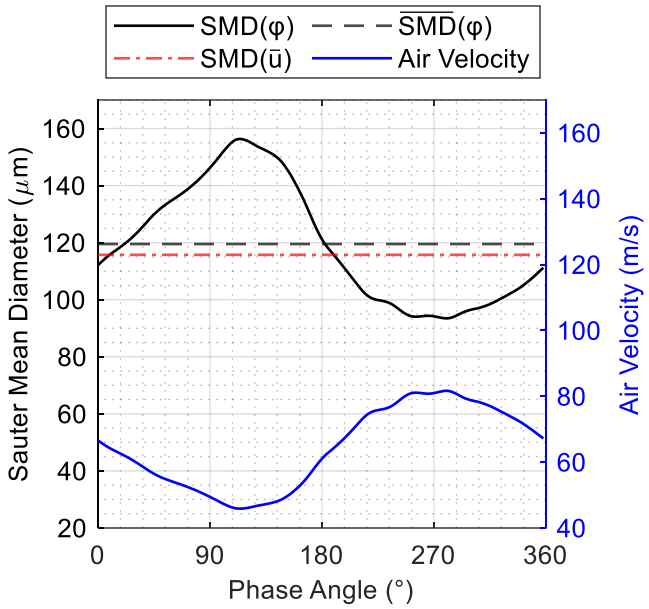

Figure 12. SMD theoretical calculation based on the measured phase averaged air velocity.

4.3.Forced flow – multiple position analysis

Having established the behavior of the spray under the acoustic forcing in one position at the centerline 40 mm downstream of the atomization edge, the final step to have a complete overview was to investigate the changes by moving away from that centerline. In total, six points were investigated along the X-axis as shown in Figure 2. In this subchapter, the oscillation of the most interesting spray characteristics along the space and time are presented.

Starting with the mean droplet velocity, Figure 13 shows the variation along the X-axis simultaneously with the oscillation in one period of the acoustic forcing. For all six measured positions, the fluctuation is almost identical; where only the average value of the velocity is changing, showing a local maximum around -5 mm. This local maximum of the mean droplet velocity was also observed in preliminary experiments under non-forced conditions in this region of the spray.

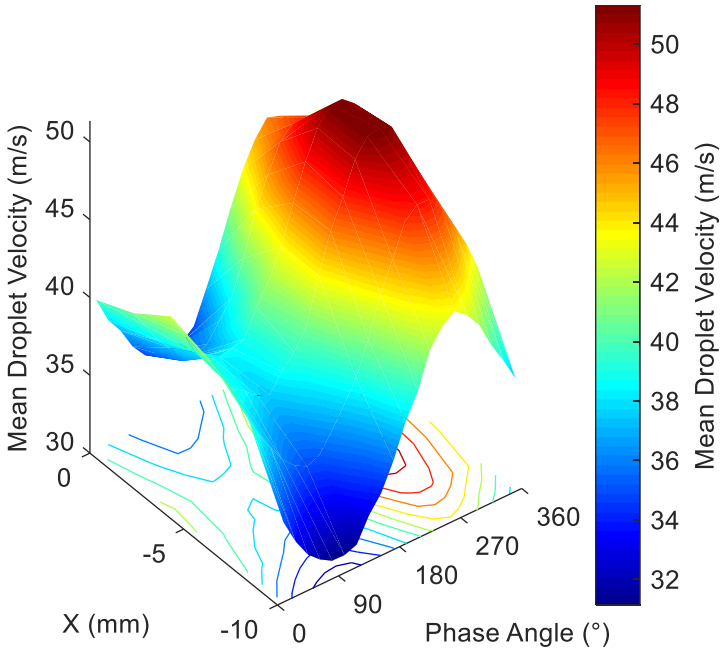

Figure 13. Mean droplet velocity oscillation in a variety of positions.

The SMD shown in Figure 14 seems almost constant along the X-axis, with a slight local minimum at a position of around -5 mm, where the velocity showed a local maximum. Interesting is that the amplitude of the oscillation of the SMD remains the same in all positions, exactly like the velocity oscillation.

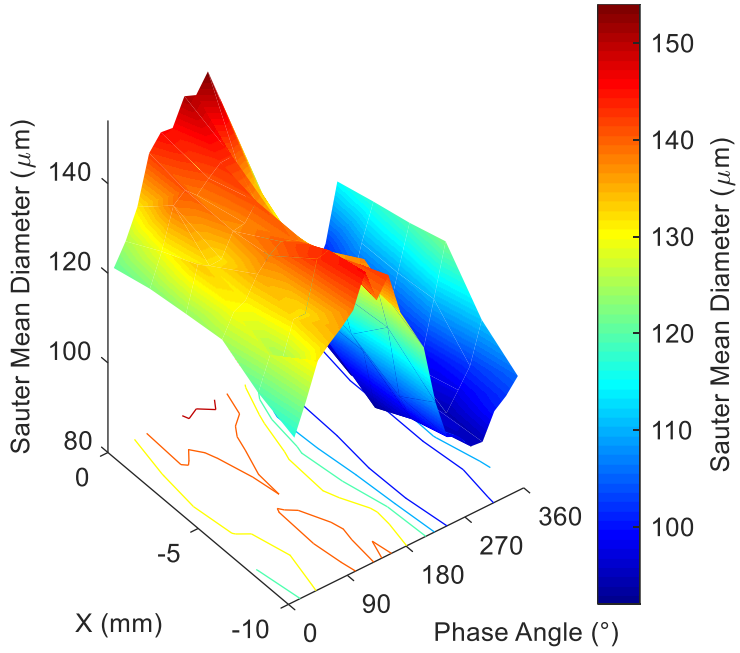

Figure 14. SMD oscillation in a variety of positions.

Finally, the number of droplets passing through the measurement volume during the period of the acoustic forcing is shown in Figure 15 for the six selected positions. Around -5 mm, where the droplet velocity has a local maximum, a larger amplitude of the droplet number oscillation is observed.

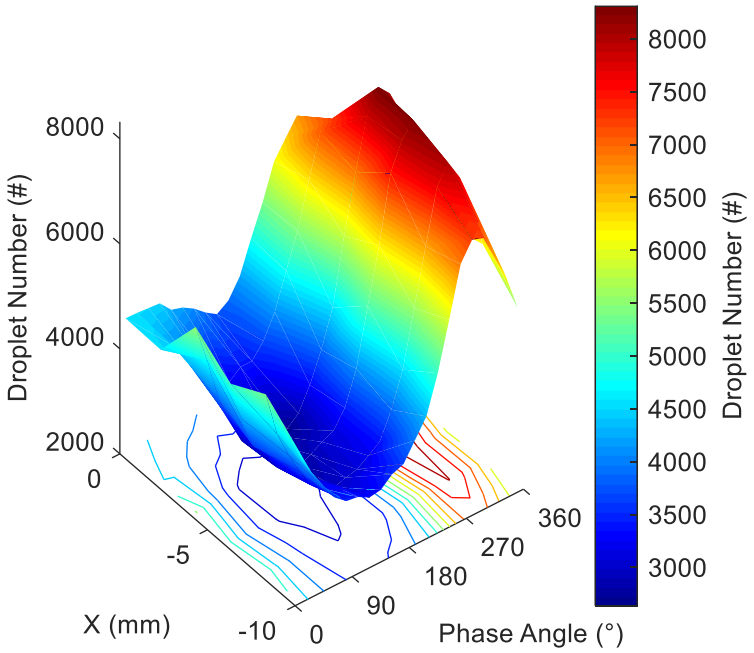

Figure 15. Droplet number oscillation in a variety of positions.

5.Conclusion

The spray characteristics of a planar prefilming nozzle were measured under atmospheric conditions by means of Phase Doppler Anemometry under pulsating flow conditions in a variety of positions along the axis where the angle of the spray increases. A part of the total airflow passes through a siren, a device which introduces oscillations of a certain frequency in the flow so that the spray is characterized under unsteady conditions. The flow field oscillation generated by the siren was investigated by hot-wire CTA measurements, and the resulting air velocity signal was post-processed using the Fast Fourier Transform, which provided information about the oscillation frequency of the velocity and its amplitude. The forced flow experiment was performed with the siren motor rotating at 900 RPM, resulting in an oscillating airflow at 120.16 Hz.

The air velocity signal was phase-averaged according to the determined frequency, which shows that a very clear and periodic oscillation was indeed developed. A similar post-processing technique in order to phase-average the spray characteristics measured by PDA, namely mean

diameter, SMD, and mean drop velocity, was applied. The discussion of the experimental results can be summarized in the following conclusions:

- The mean diameter, SMD, and mean droplet velocity indeed oscillate at the same frequency as the air velocity.

- The SMD measured for the average air velocity in a non-forced flow experiment matches the corresponding average SMD from Figure 11.

- The SMD can be calculated from the correlation proposed by Gepperth et al. (Gepperth et al., 2012), using the phase averaged air velocity from Figure 6, as it was shown in Figure 12. Its average value is slightly higher than the SMD of the average air velocity calculated from Equation 3, replicating the experimental observations from Figure 11.

- The SMD and the mean diameter of the droplets have a natural shift of approximately 180° compared to the droplet velocity. This shift matches the numerical calculation of the SMD from Equation 3 presented in Figure 12.

- The droplet velocity along the X-axis reaches a local maximum at -5 mm, where the droplet number crossing the PDA measurement volume has its maximum amplitude. The SMD on the other hand does not critically vary in the measured positions.

The resulting response of the spray characteristics can be exploited in thermoacoustic models using machine learning in order to predict the instabilities on a combustion chamber of a real aircraft engine. Since this response is evident on the tested frequency of 120.16 Hz, further research activities on a variety of excitation frequencies will provide a better overview of the phenomenon and a larger database for the prediction models.

Acknowledgments

This project has received funding from the European Union's Horizon 2020 research and innovation programme under the Marie Sklodowska-Curie Agreement 766264 (MAGISTER). The authors would like to thank the Institute of Thermal Turbomachinery (ITS) in KIT for the expertise regarding the planar prefilming airblast atomizer model, as well as the Chair of Thermodynamics in TUM for manufacturing, testing and providing the pulsation device. Finally, the authors would like to gratefully acknowledge the financial support by the German Research Foundation (DFG) for measuring equipment under HBFG programme INST 121384/178-1 FUGG.

References

Chaussonnet, G. *et al.*, Time-Response of Recent Prefilming Airblast Atomization Models in an Oscillating Air Flow Field, *Journal of Engineering for Gas Turbines and Power*, vol. **139**, no. 12, 121501 1-9, 2017. DOI: 10.1115/1.4037325

Collins, L.R. and Keswani, A., Reynolds number scaling of particle clustering in turbulent aerosols, *New Journal of Physics*, vol. **6**, no. 119, 1-17, 2004. DOI: 10.1088/1367-2630/6/1/119

Déjean, B., Berthoumieu, P., and Gajan, P., Eds., *Experimental study on the influence of the liquid and air thicknesses on a planar air-blasted liquid sheet*, 2013.

DeLaat, J.C. and Paxson, D.E., Eds., *Characterization and simulation of the thermoacoustic instability behavior of an advanced, low emissions combustor prototype*, 2008.

Dowling, A.P. and Stow, S.R., Acoustic Analysis of Gas Turbine Combustors, *Journal of Propulsion and Power*, vol. **19**, no. 5, 2003. DOI: 10.2514/2.6192

Eckstein, J. *et al.*, Forced Low-Frequency Spray Characteristics of a Generic Airblast Swirl Diffusion Burner, *Journal of Engineering for Gas Turbines and Power*, vol. **127**, no. 2, pp. 301–306, 2005. DOI: 10.1115/1.1789515

Gajan, P. *et al.*, Investigation of Spray Behavior Downstream of an Aeroengine Injector with Acoustic Excitation, *Journal of Propulsion and Power*, vol. **23**, no. 2, pp. 390–397, 2007. DOI: 10.2514/1.22394

Gepperth, S., Müller, A., Koch, R., and Bauer, H., Eds., *Ligament and Droplet Characteristics in Prefilming Airblast Atomization*, 2012.

Gurubaran, R.K., Sujith, R.I., and Chakravarthy, S.R., Characterization of a prefilming airblast atomizer in a strong swirl flowfield, *Journal of Propulsion and Power*, vol. **24**, no. 5, pp. 1124–1132, 2008. DOI: 10.2514/1.35012

Inamura, T. *et al.*, Eds., *Spray Characteristics of Prefilming Type of Airblast Atomizer*, 2012.

Müller, A. *et al.*, Eds., *Performance of Prefilming Airblast Atomizers in Unsteady Flow Conditions*, 2006.